Table of Contents, University of California, Berkeley

I. FISCHER-TROPSCH SYNTHESIS ON IRON CATALYSTS

1. Background

1.1. Structure and Function of Active Phases in Fischer-Tropsch Synthesis

Fe-based oxides have been used as commercial catalysts for Fischer-Tropsch synthesis (FTS) to produce a large variety of paraffin and olefin products, ranging from methane to high molecular weight waxes [1]. During activation in synthesis gas and subsequent FTS reaction, several phases including metallic iron, iron carbides and iron oxides can co-exist at steady-state conditions [2-5]. The relative amounts of these phases depend on various activation and reaction conditions, which also lead to different catalytic performance. Some researchers [6] have proposed that surface iron atoms are responsible for FTS activity, while others have considered surface carbides or a mixture of carbides [7,8] with metallic iron [9] to be the active phase. There are also some reports that suggest that magnetite Fe_3O_4 is the active FTS phase [10-12]. Although these studies have each provided some evidence to support their specific proposals about the active phase, the available information remains phenomenological and sometimes contradictory, and a direct method to identify the active phase during reaction and to count the number of active sites has remained elusive.

We have tried to establish more conclusively the active phases required for FTS in the previous studies [22]. In this reporting period, we have started site titration measurements of the density of active sites. The method used is H_2, CO and H_2/CO chemisorption/desorption using on-line mass spectrometry. We monitored the gas phase concentrations of the desorbed species and we studied the adsorption mechanism of H_2 and CO on these active sites. In addition, we have prepared K- and Re-promoted Fe-Si catalysts and investigated the reduction and carburization process and catalytic activity as in our search for alternative catalysts for FTS reaction.

1.2. Effects of Zn, K and Cu on Fe Oxides

Many components have been added to Fe catalysts in order to improve their mechanical and catalytic properties. Our previous studies have shown that Zn, K and Cu [13-15] promote the catalytic properties of Fe oxides. Zinc oxide, as a non-reducible oxide at FTS conditions, appears to stabilize the surface area of Fe oxide. Alkali, as a modifier of the adsorption enthalpies of H_2 and CO, increases the selectivity to desired C_{5+} products. Copper promotes the carburization processes and decreases the temperature required for the activation of iron oxide precursors. We have prepared a series of Zn and Fe co-precipitated oxides with a range of Zn/Fe atomic ratios and then introduced varying amounts of K and Cu. We have examined the surface area, bulk structure, required reduction and carburization temperatures, as well as the catalytic behavior of these catalysts, in order to identify optimum Zn/Fe ratios and Cu and K contents that give maximum site density and catalytic activity.

1.3 Effects of K and Re on Fe-Si Oxides

In this reporting period, we have prepared and investigated the reduction and carburization behavior as well as the catalytic activity of K- and Re-promoted oxides based on Fe-Si oxide precursors provided by Dr. Burtron Davis at the Center for Applied Energy Research of the University of Kentucky. Si acts as a structural promoter and it stabilizes a higher surface area. Our previous studies of K on Fe-Zn-Cu oxides have shown that K increases FTS and water-gas shift activity [19]. The same effects of K are expected on Fe-Si oxides. Also, K was added in order to increase wax and alkene yields, while decreasing the production of undesirable methane. Re, which is a not a good water-gas shift catalyst, was introduced because we are attempting to explore the possibility of using Re as a substitute for Cu.

2. Synthesis Procedures

2.1 Fe-Zn-K-Cu Oxides

Fe-Zn-K-Cu catalysts were prepared by co-precipitation of iron and zinc nitrates followed by the impregnation of an aqueous solution of potassium carbonate and copper nitrate using incipient wetness methods. The detailed preparation procedure was presented in our previous report [18].

2.2. Fe-Si-K or Fe-Si-Re Oxides

The Fe-Si oxide precursors, which were provided by Dr. Burtron Davis' group at the Center for Applied Energy Research of the University of Kentucky, were prepared by continuous precipitation of amorphous ferric oxyhydroxide from aqueous Fe nitrate and concentrated ammonium hydroxide at pH 9.5. Hydrolyzed tetraethyl orthosilicate was added to the Fe nitrate solution to give the desired silicon level (Si/Fe=0.046). The precipitates were then washed, filtered and dried at 393 K. The preparation detail of precipitated Fe-Si (Si/Fe=0.046) oxide precursors are presented elsewhere [16]. The Fe-Si oxide precursor was treated in air at 350 ^{o}C for 4 h. The air-treated sample was promoted with 1.4 at. % K using a K_2CO_3 solution (0.16 M) and incipient wetness impregnation protocols and then dried at 373 K. A similar incipient wetness method was used in order to promote samples with 0.05~2 at. % Re using perrhenic acid (Aldrich, 99+%) solutions (10 mg/ml). Fe-Si-Re oxides were dried at 293 K without calcination in order to prevent sublimation of Re_2O_7 at 523 K. The dried Fe-Si-K oxide was treated in dry air at 350 ^{o}C for 4 h. All the dried materials were then pelletized to 80-140 mesh before FTS reactions.

3. Catalyst Characterization

3.1. Protocols for the Characterization of Fe-based FTS Catalysts

This research program addresses the synthesis and the structural and catalytic characterization of active sites in Fe-based catalysts for FTS. We have designed a matrix of samples that contains a systematic range of multicomponent catalysts in order to determine the number and type of surface sites present on fresh catalysts and on samples during and after FTS reaction (Table 1.1). Our objective is to develop rigorous relationships between the synthesis methods, the resulting catalyst structures, and their function in FTS reactions.

3.2 In-situ X-ray Absorption (XAS) Measurements of Structural Evolution in FTS

During this reporting period, we have continued our X-ray absorption studies at the Stanford Synchrotron Radiation Laboratory (SSRL) with emphasis on the Fe K-edge measurements on K and Cu promoted samples during FTS reactions. During this quarter, we have finished all the *in-situ* X-ray absorption studies of the structural evolution during initial and long-term FTS reaction on Fe-Zn-K-Cu oxides. The experimental methods have been described in previous quarterly reports [22].

Figure 1.1 shows the structural evolution of precipitated Fe_2O_3-Cu during FTS at 523 K for 14 h. The linear combination fits X-ray absorption near edge spectroscopy (XANES) of standard Fe_2O_3, Fe_3O_4, and Fe_xC compounds showed that the concentration of Fe_2O_3 decreased significantly as a function of time on stream while the concentration of Fe_3O_4 increased and then decreased with time on stream. The concentration of Fe_xC increased monotonically as the FTS reaction proceeded. The compositional evolution of Fe_2O_3, Fe_3O_4, and Fe_xC fits the pattern of a sequential reduction-carburization reaction. This observation confirmed our previous studies of the temperature-programmed reaction of Fe_2O_3-Cu in CO, which showed that Fe_2O_3 is first converted to Fe_3O_4 and then to Fe_xC. Our previous reaction transient studies showed that most of the reduction/carburization takes place during the initial exposure of the catalyst to synthesis gas (<1 h) and that the FTS rates reached steady-state values during this initial exposure time [22]. Therefore, it appears that the FTS reaction rates reflect only the surface layers of the catalyst, which have already reached the steady-state composition, even as Fe_3O_4 continues to reduce and carburize to Fe_xC during FTS reactions.

Table 1.1. Matrix of samples and characterization methods for FTS reaction

Nominal Composition of the Catalysts			Characterization Before and After FTS	FTS reaction
Zn/Fe mole ratio	K/(Fe+Zn) (at.%)	Cu/(Fe+Zn) (at.%)		
0	0	0	XRD Surface area In-situ XAS H_2-TPR CO-TPR	Effect of reaction condition 220 °C 21.4 atm 235 °C 21.4 atm 270 °C 5 atm Effect of CO_2 addition Isotopic studies
		1		
	2	0		
		1		
		2		
	4	1		
0.05	0	0		
	2	1		
	4	2		
0.1	0	0		
		1		
	2	0		
		1		
		2		
	4	1		
0.2	0	0		
	2	1		
	4	2		
0.4	0	0		
		1		
	2	0		
		1		
		2		
	6	1		
Si/Fe	K/Fe (at.%)	Re/Fe (at.%)		
0.046	0	1		
		2		
	1	0		

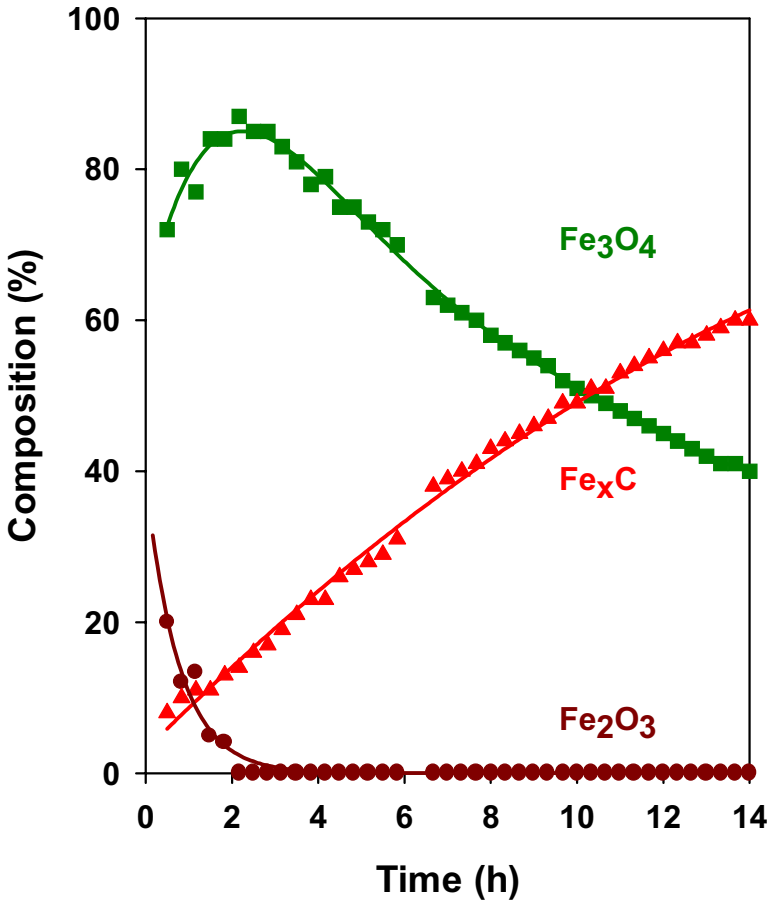

Figure 1.1 I*n-situ* XAS phase compositions (1 mg Fe_2O_3-Cu, Cu/Fe=0.01) as a function of time in synthesis gas (H_2/CO=2, GHSV= 6000) at 523 K.

When a small amount of K (K/Fe=0.02) is added to the above Fe_2O_3-Cu sample, not only the concentration of Fe_2O_3, but also that of Fe_3O_4 decreased markedly as a function of time, while the concentration of Fe_xC increased rapidly and reached a very high stable state concentration (90%) after 4 h on stream (Figure 1.2). The entire reduction and carburization process is significantly shortened where K is present. This appears to reflect the ability of K to increase the rate of carburization, as we have previously found in temperature-programmed reduction/carburization in CO [19]. The synergistic combination of Cu and K increases markedly carbruization rates.

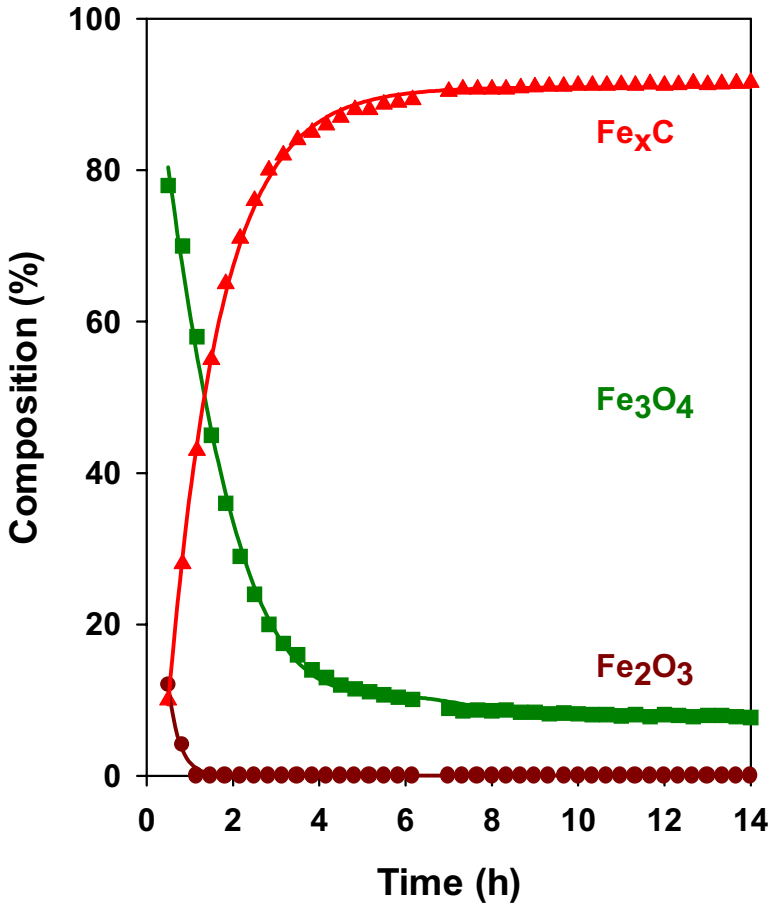

Figure 1.2 I*n-situ* XAS phase compositions (1 mg Fe_2O_3-Cu-K, Cu/Fe=0.01, K/Fe=0.02) as a function of time in synthesis gas (H_2/CO=2, GHSV= 6000) at 523 K.

3.3. H_2 and CO chemisorption on Fe Oxides

Precipitated Fe oxides (0.2 g) were treated in flowing He (100 cm^3/min) at temperatures up to 573 K and then cooled down to 523 K. The He stream was switched to a flow of 60% synthesis gas (H_2/CO=2) in Ar (total flow rate 100 cm^3/min) at 523 K. After exposure to synthesis gas for 1 h, the synthesis gas stream was switched back to He and maintained at 523 K for an additional 1 h before quenching to ambient temperature. The quenching process was done by removing the furnace from the reactor and letting the reactor cool to ambient temperature. A flow of 40% H_2, or 20% CO or 60% synthesis gas (H_2/CO=2) balanced by Ar (total flow rate 100 cm^3/min) was passed through the samples for 0.5 h in order to carry out the adsorption. Physisorbed species were removed after 0.5 h in flowing Ar (flow rate 100 cm^3/min) and the chemisorbed species were monitored in a temperature-programmed desoption (TPD) mode (10 K/min) using mass spectrometry.

In our last quarterly report, our mass spectroscopy and X-ray absorption spectroscopy studies of the samples during the FTS reaction showed that this sample consists of bulk Fe_3O_4 and surface Fe carbides after FTS reaction at 523 K for 1 h. After chemisorption, H_2, CO and CO_2 were the only detectable desorption species. No measurable amounts of H_2O or hydrocarbons were observed during temperature-programmed desorption in Ar.

3.3.1. H_2 desorption

Figures 1.3, 1.4 and 1.5 shows the H_2, CO and CO_2 desorption rates as a function of temperature after chemisorption of each of the titrants (H_2, CO or H_2/CO) absorbents on precipitated Fe_2O_3 after FTS reaction at 523 K for 1 h. Table 1.2 shows the quantitative analysis of the amounts desorbed during TPD in Ar up to temperatures of 800 K. Figure 1.3a shows the sample without adsorbing any titrants after He treatment at 523 K; a broad H_2 desorption peak appears at 500-800 K. This indicates that some hydrogen atoms (8.8 μmol H_2/g-atom Fe) remain strongly adsorbed on Fe carbide surfaces, and that they are not removed by flowing He at 523 K. After adsorbing hydrogen at ambient temperature for 0.5 h, the subsequent TPD shows that H_2 desorption (Figure 1.3b) begins at ~100 K lower than on the sample without H_2 chemisorption (Figure 1.3a), and that there are 7.9 μmol H_2/g-atom Fe more hydrogen atoms adsorbed on the Fe carbide surface. When using CO as the titrants (Figure 1.3c), the H_2 desorption peak (9.1 μmol H_2/g-atom Fe) unchanged, suggesting that these strongly adsorbed H-atoms are not accessible by CO at ambient temperature. When using synthesis gas (H_2/CO=2) as titrant, the amount of adsorbed hydrogen atoms (13.8 μmol H_2/g-atom Fe) is smaller than when only using H_2 as titrant (16.7 μmol H_2/g-atom Fe), indicative of competitive adsorption between H_2 and CO.

Table 1.2 Quantitative analysis of desorption species during TPD in Ar at temperatures up to 800 K

Titrant	Amount desorbed (μmol/g-atom Fe)			
	H_2	CO	CO_2	Total ($CO+CO_2$)
He	8.8	7.9	4.3	12.2
H_2	16.7	3.8	7.8	11.6
CO	9.1	13.1	7.1	20.2
H_2/CO	13.8	11.8	4.1	15.9
H_2-He	13.5	3.9	1.9	5.8

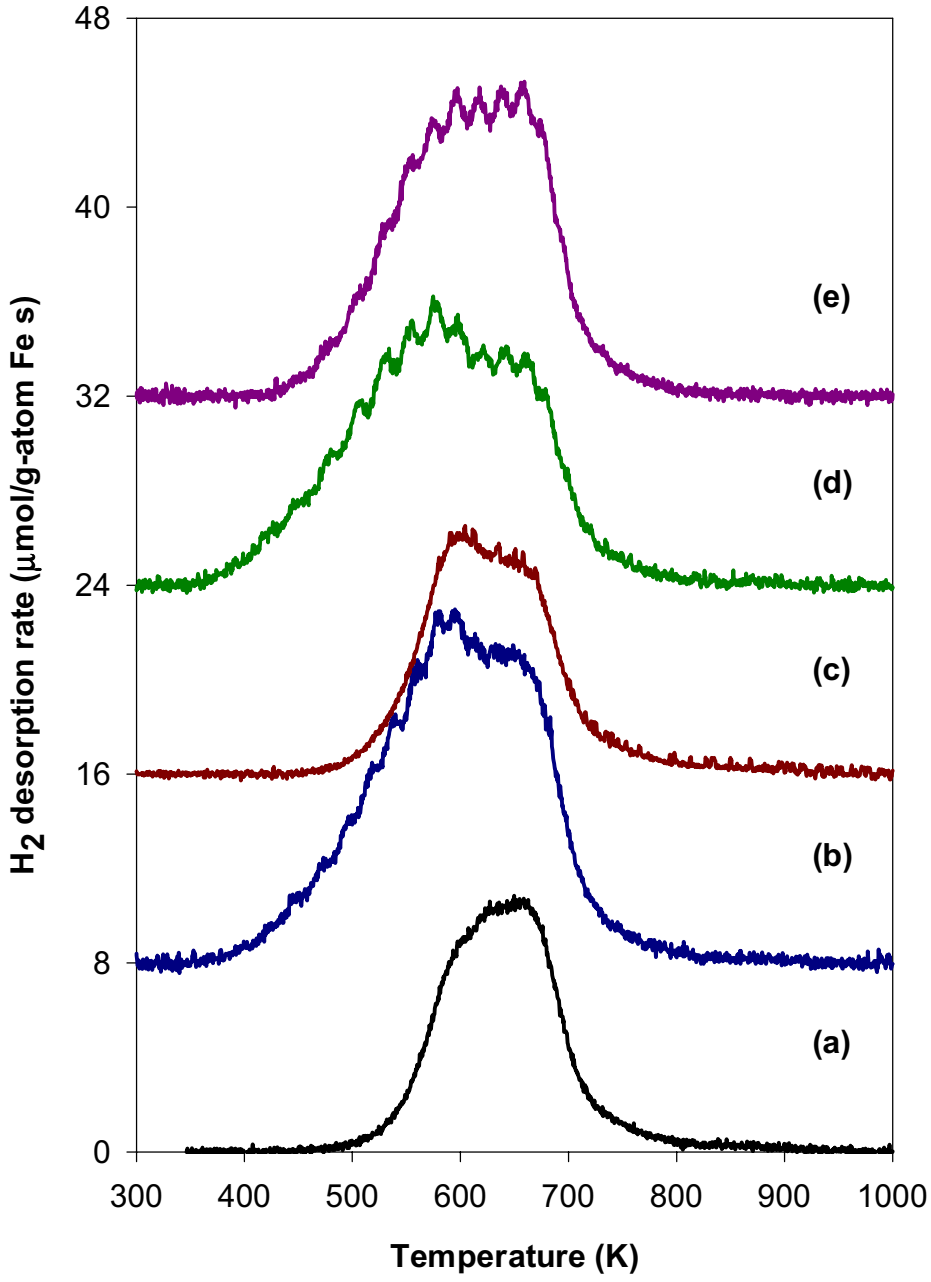

Figure 1.3 Temperature-programmed desorption of H_2 after FTS reaction and chemisorption. (0.2 g Fe_2O_3, FTS condition: 523 K, H_2/CO=2, total flow rate 100 cm_3/min)
(a): FTS 1 h, quenched in He, TPD in Ar;
(b): FTS 1 h, quenched in He, H_2 chemisorption at room temperature, TPD in Ar;
(c): FTS 1 h, quenched in He, CO chemisorption at room temperature, TPD in Ar;
(d): FTS 1 h, quenched in He, syngas chemisorption at room temperature, TPD in Ar.
(e): FTS 1 h, H_2 treatment 1 h, quenched in He, TPD in Ar.

3.3.2 CO and CO_2 desorption

Figures 1.4 and 1.5 show the CO and CO_2 desorption rates as a function of temperature after chemisorption of each titrant on precipitated Fe_2O_3 after using such analysis in FTS reaction at 523 K for 1 h. CO and CO_2 desorb simultaneously, implying that the desorption of CO is the rate determining step. When CO desorbs, it may react readily with distant adsorbed O species, forming CO_2. Figures 1.4a and 1.5a show the desorption peaks of CO and CO_2 immediately after FTS reaction and before chemisorption. The total amount of adsorbed carbon species is 12.2 μmol C/g-atom Fe. When chemisorbing H_2, the amount of desorbed CO (Figure 1.4b) decreases and the amount of CO_2 (Figure 1.5b) increased. Although it is not clear why much more CO_2 desorbs than CO, the total amount of desorbed carbon species (11.6 μmol C/g-atom Fe) is similar to that on the sample before H_2 chemisorption. This indicates that H_2 chemisorption at ambient temperature does not scavenge adsorbed carbon species. Figures 1.4c and 1.5c show the desorption of CO and CO_2 after CO chemisorption. Compared with Figure 1.3c, the total amount of desorbed CO and CO_2 (8.0 μmol C/g-atom Fe) is similar to the amount of adsorbed hydrogen, which is 7.9 μmol H_2/g-atom Fe. This means that the total accessible adsorption sites on Fe carbides is ~8 μmol/g-atom Fe, and H_2 and CO competitively adsorb on the same Fe sites. Since H_2 adsorbs dissociatively on Fe sites, the almost equal amount of adsorbed H_2 and CO indicates that one adsorbed CO molecule occupies two Fe sites. When adsorbing synthesis gas, the total amount of adsorbed CO and CO_2 (15.9 μmol C/g-atom Fe) is about 3.7 μmol C/g-atom Fe higher than the sample without chemisorption. Including the amount of adsorbed hydrogen (13.8-8.8=5 μmol H_2/g-atom Fe), the total amount of adsorbed H_2 and CO is 8.7 μmol H_2 or C/g-atom Fe, which is slightly higher than the accessible Fe sites. This suggests that some of CO is molecularly adsorbed on Fe sites in the presence of H_2.

All the above chemisorptions were carried out after exposure of the sample to 60 % synthesis gas (H_2/CO=2) in Ar at 523 K for 1 h followed by He treatment at the same temperature for an additional 1 h. In the next set of experiments, we switched the flow to 40 % H_2 in He for 1 h instead of using pure He. Figures 1.3e, 1.4e and 1.5e show the desorption rates of H_2, CO and CO_2 as a function of temperature. The amount of adsorbed hydrogen atoms is ~4.7 (μmol H_2/g-atom Fe) higher than the sample without H_2 treatment, while the total amount of adsorbed CO and CO_2 is ~6.3 (μmol C/g-atom Fe) smaller than the sample without H_2 treatment. This suggests that some of the adsorbed carbon species reacted with H_2 during treatment at 523 K, while more strongly adsorbed carbon species were left behind. Comparing Figure 1.3a with Figure1.3e, the difference between these two curves (4.7 μmol/g-atom Fe) reflects sites that on which H_2 and CO coadsorb during FTS reaction. The scavenged carbon sites (6.3 μmol C/g-atom Fe) is more than hydrogen readsobed sites (4.7 μmol H_2/g-atom Fe), confirming that some of the carbon species absorb molecularly in the presence of H_2.

In a conclusion, H_2 and CO competitively adsorb on Fe sites. Similar to H_2, CO occupies two Fe sites while chemisorbing alone. In the presence of H_2, some CO absorbs molecularly on Fe sites.

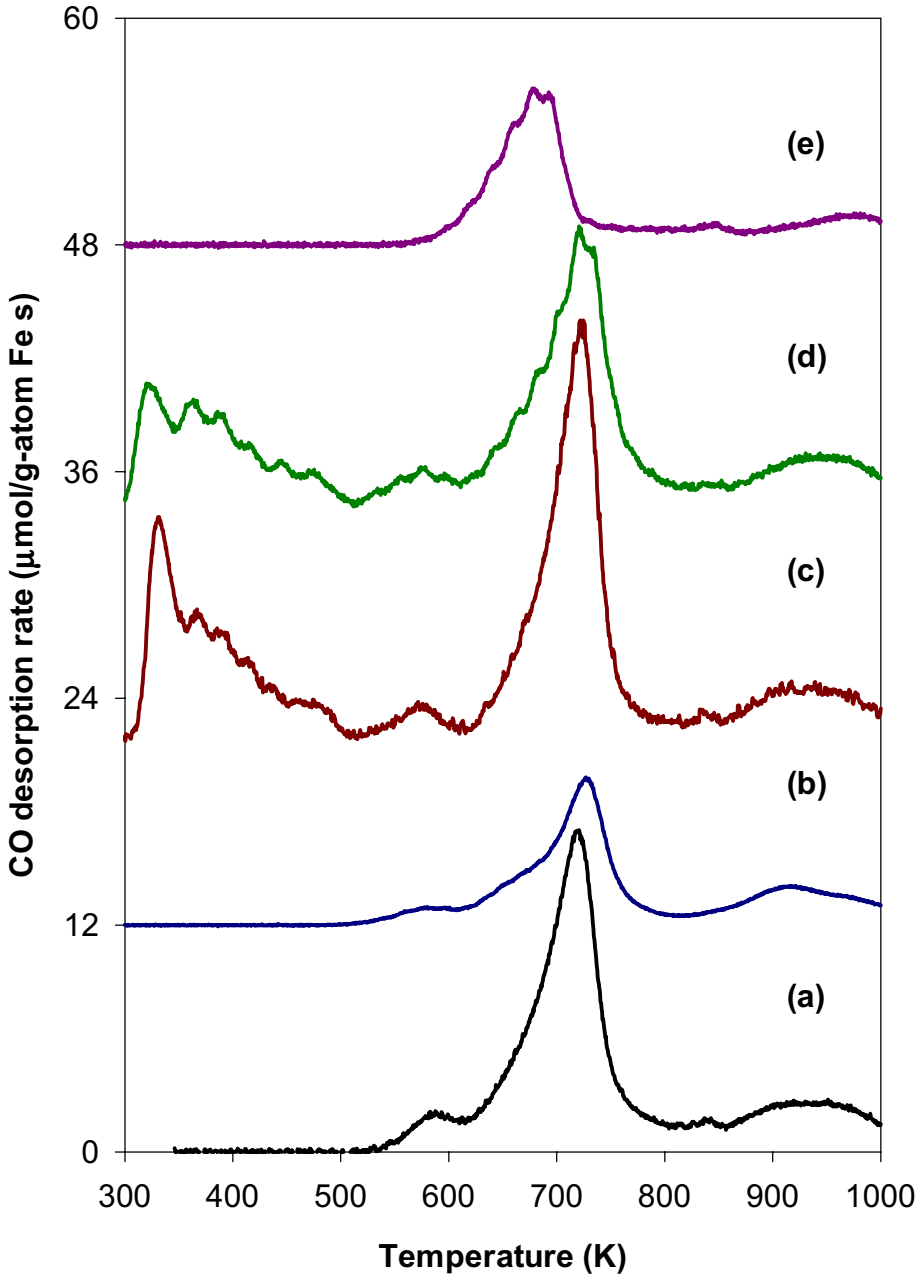

Figure 1.4 Temperature-programmed desorption of CO after FTS reaction and chemisorption. (0.2 g Fe_2O_3, FTS condition: 523 K, H_2/CO=2, total flow rate 100 cm_3/min)
(a): FTS 1 h, quenched in He, TPD in Ar;
(b): FTS 1 h, quenched in He, H_2 chemisorption at room temperature, TPD in Ar;
(c): FTS 1 h, quenched in He, CO chemisorption at room temperature, TPD in Ar;
(d): FTS 1 h, quenched in He, syngas chemisorption at room temperature, TPD in Ar.
(e): FTS 1 h, H_2 treatment 1 h, quenched in He, TPD in Ar.

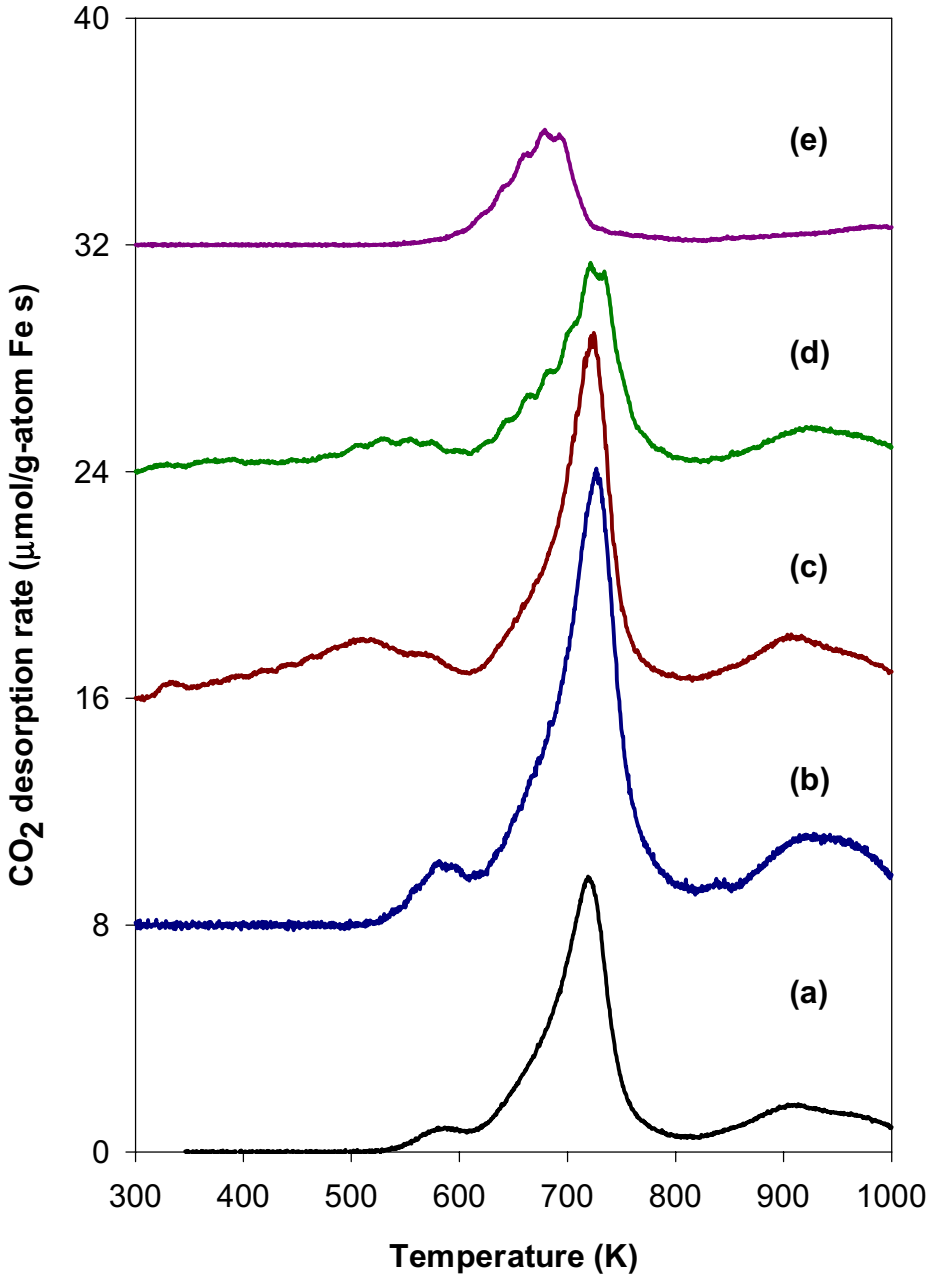

Figure 1.5 Temperature-programmed desorption of CO_2 after FTS reaction and chemisorption. (0.2 g Fe_2O_3, FTS condition: 523 K, $H_2/CO=2$, total flow rate 100 cm_3/min)
(a): FTS 1 h, quenched in He, TPD in Ar;
(b): FTS 1 h, quenched in He, H_2 chemisorption at room temperature, TPD in Ar;
(c): FTS 1 h, quenched in He, CO chemisorption at room temperature, TPD in Ar;
(d): FTS 1 h, quenched in He, syngas chemisorption at room temperature, TPD in Ar.
(e): FTS 1 h, H_2 treatment 1 h, quenched in He, TPD in Ar.

3.4. Reduction and Carburization of Fe-Si-K or Fe-Si-Re Oxides

Table 1.3 shows the surface area of K and Re promoted Fe-Si oxide. After drying at 393 K, the Fe-Si oxide has a surface area of 190 m^2/g, Fe-Si oxide does not appear to sinter after treatment in air at 623 K for 4 h. SiO_2 acts as a structural promoter, leading to higher surface area on Fe-Si oxide than on Fe oxide (182 vs 52 m^2g^{-1}). The impregnation of K and Re slightly decreases the surface area of the Fe-Si oxide. X-ray diffraction measurements of precipitated Fe-Si oxides showed that Fe-Si and promoted Fe-Si oxides are amorphous, suggesting that FeO_x-SiO2 mixed oxides may be present and that they prevent crystallization of Fe_2O_3 or Fe_3O_4.

Table 1.3 Comparison of the surface area of Fe and Fe-Si oxides

Surface area	Fe	Fe-Si	Fe-Si-K	Fe-Si-Re
m^2/g	52	182	170	171

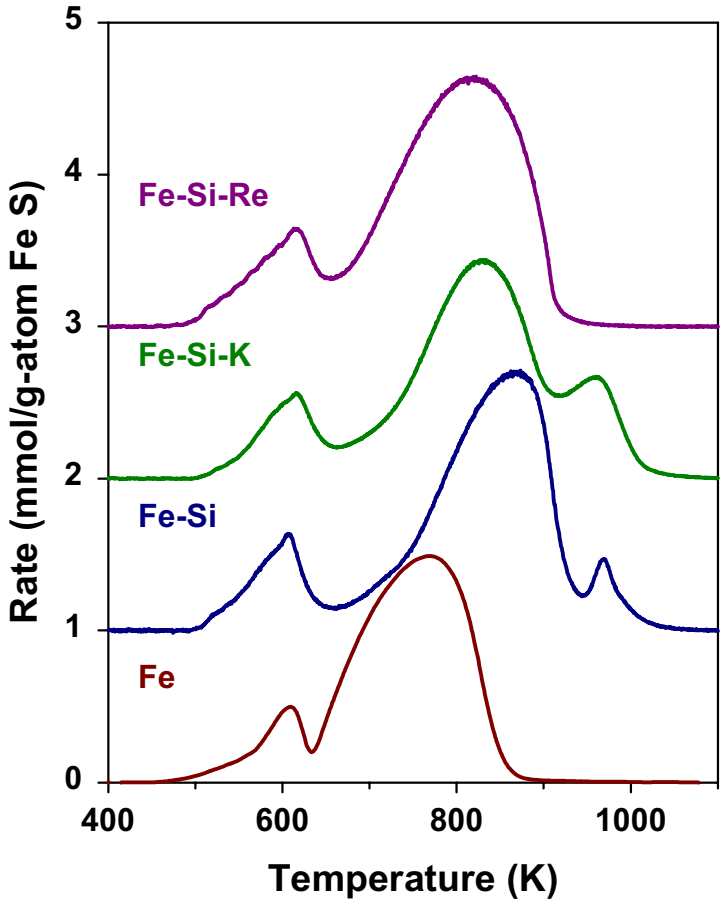

Figure 1.6. TPR of Fe-Si samples in H_2. (0.2 g samples; 10 ^oC/min ramping rate; Si/Fe=0.046, K/Fe=0.014, Re/Fe=0.01, 100 cm^3/min 20% H_2/Ar.)

Figure 1.6 shows the oxygen removal rates of Fe_2O_3, Fe-Si oxides, and promoted Fe-Si samples in H_2. Fe-Si oxides show similar reduction profiles as Fe_2O_3. i.e., Fe_2O_3 is first reduced to Fe_3O_4 and then to metallic Fe. The presence of Si does not appear to influence the reduction from Fe_2O_3 to Fe_3O_4. However, it significantly inhibits the reduction from Fe_3O_4 to metallic Fe. This suggests that the removal of oxygen from Fe_3O_4 may require the cleavage of Fe-O-Si bonds. The strong interaction between Fe and Si inhibits Fe_3O_4 reduction. K addition to Fe-Si slightly decreases the reduction temperature from Fe_3O_4 to Fe, suggestive of the titration of K with Si because of the basicity of K. Re increases the reduction rate from Fe_3O_4 to Fe because of the reduction of Re_2O_7 to Re at higher temperatures (>580 K); the later can provide H_2 dissociation sites, as Cu was previously shown to do in Fe-Zn-Cu catalysts [22].

Temperature-programmed reduction and carburization of Fe-Si oxides in CO have also been carried out. A typical TPSR of Fe-Si oxide in CO follows a similar reduction/carburization profile as for Fe_2O_3. Generally, the reduction/carburization of the oxides proceeds in three steps: Fe-Si oxide is first reduced to Fe_3O_4; Then, Fe_3O_4 is reduced to metallic Fe followed by carburization to Fe carbides. The excess free carbon formed at higher temperature (>800 K) via the Boudouard reaction. Figure 1.7 shows the reduction and carburization rate of Fe-Si oxides as function of temperature in CO. The Fe-Si oxide reduces and carburizes at slightly lower temperatures than Fe_2O_3. The addition of K evidently decreases the temperature required to reduce and carburize Fe-Si oxide. This is apparently because K titrates Si or the other way around that weakens the interaction between Fe and Si. Re, on the other hand, does not appear to have much effect on the reduction and carburization of Fe-Si oxides. This may be because Re_2O_7 is not reduced to Re at lower temperatures and Re does not dissociate CO. Therefore, Re may be unable to help the reduction by CO at lower temperatures or the subsequent carburization of Fe_3O_4 to FeC_x.

3.5. Isothermal Switch Transient Studies of Fe-Si Oxides in Synthesis Gas

A rapid switch transient method with mass spectrometric analysis was used in order to determine the initial reduction and carburization behavior of Fe oxides, as well as their catalytic CO hydrogenation properties in H_2/CO mixtures. Typically, samples (0.2 g) were pretreated in dry air (100 cm^3/min) at temperatures up to 573 K and cooled down in He to 523 K. The He stream was switched to a flow of 60 % synthesis gas (H_2/CO=2) in Ar (total flow rate 100 cm^3/min) at 523 K. The resulting isothermal transients of CH_4, H_2O and CO_2 were monitored as a function of time using on-line mass spectrometry.

Figure 1.8 shows the isothermal transients measured at 523 K during reduction and carburization and subsequent FTS of Fe-Si oxide in synthesis gas (H_2/CO=2). Fe-Si oxide shows similar initial product transient patterns as Fe_2O_3 except that the induction period is shortened and the CH_4 formation rate is higher. CO is the preferential reductant for Fe-Si oxide in H_2/CO mixtures. The high surface area of Fe-Si oxide appears to contribute to a larger amount of oxygen removed during the induction period and to the higher FTS rates obtained from Fe-Si oxide precursors compared with Fe_2O_3.

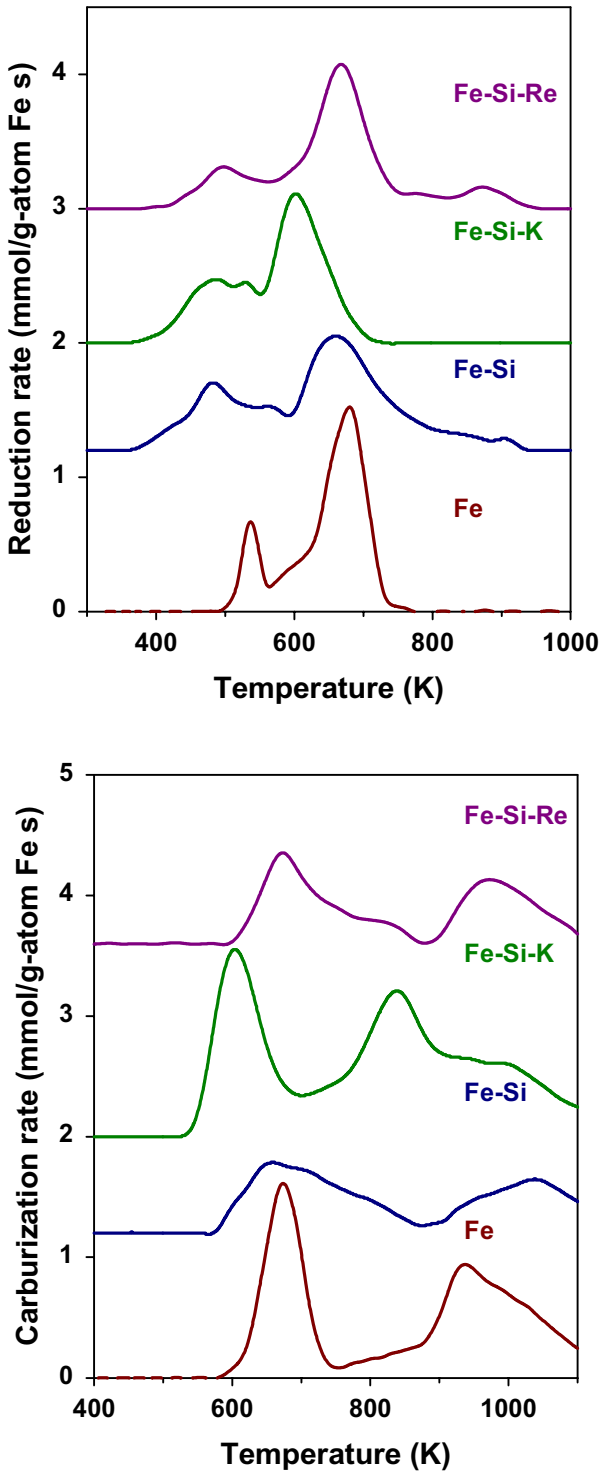

Figure 1.7 The reduction and carburization of Fe-Si oxides in CO (0.2 g samples; Si/FE=0.046, K/Fe=0.014, Re/Fe=0.01, 10 ^{o}C/min ramping rate; 100 cm^{3}/min, 20% CO/Ar).

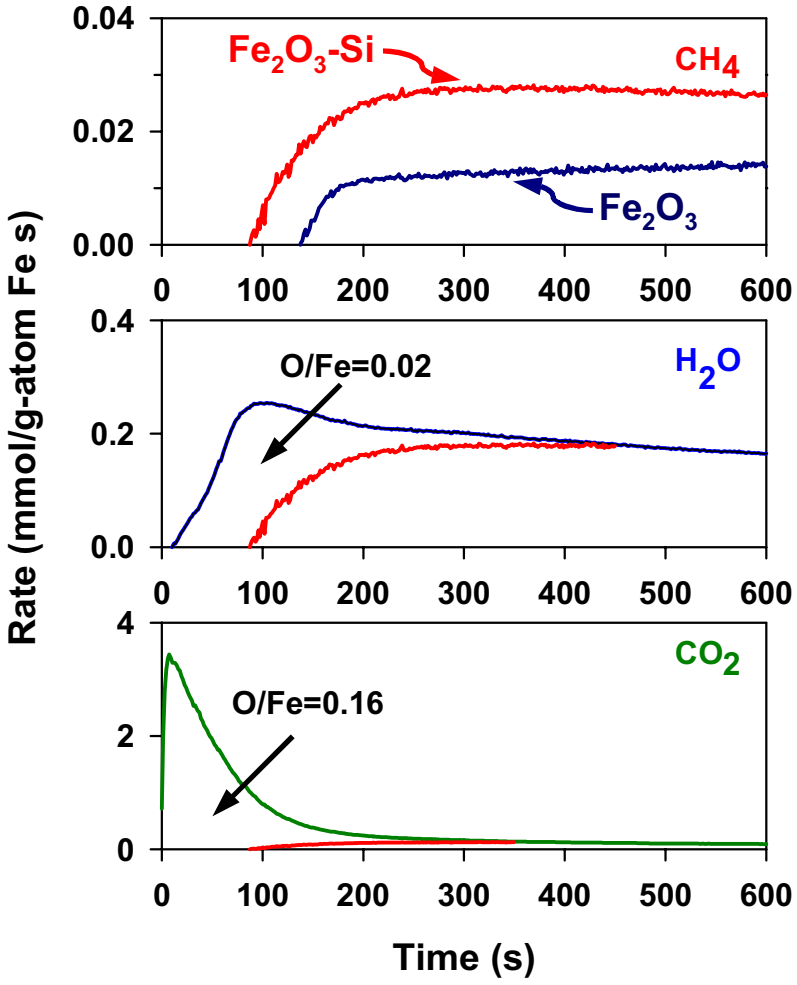

Figure 1.8 Comparison of the isothermal product transients of Fe_2O_3 and Fe-Si oixde (0.2g, Si/Fe=0.046) in synthesis gas (H_2/CO=2, 60 % synthesis gas in Ar, total flow rate 100 cm^3/min) at 523 K.

Figure 1.9 shows the isothermal transients measured at 523 K during reduction and carburization and subsequent FTS of Fe-Si-K oxide in synthesis gas (H_2/CO=2). Fe-Si-K oxide shows almost the same initial product transient pattern to that of Fe-Si oxide except that the induction period is slightly shortened and CH_4 formation rates are slightly higher. Addition of K to Fe-Si does not show as significant a promotion effect as the effect we observed previously on Fe_2O_3. This indicates that the titration of K with Si may decrease considerably the concentration and thus the chemical effects of K on the FTS reaction.

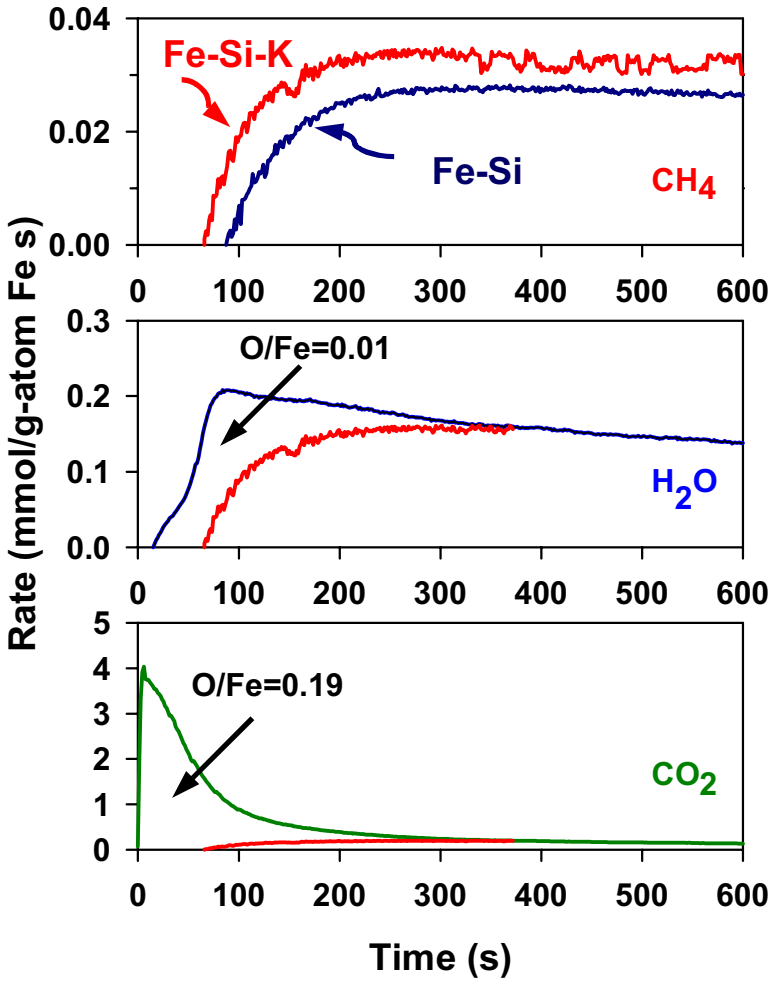

Figure 1.9 Comparison of the isothermal product transients of Fe_2O_3 and Fe-Si-K oxide (0.2g, Si/Fe=0.046, K/Fe=0.014) in synthesis gas (H_2/CO=2, 60 % synthesis gas in Ar, total flow rate 100 cm^3/min) at 523 K.

Figure 1.10 shows the isothermal transients measured at 523 K during reduction and carburization and subsequent FTS of Fe-Si-Re oxide in synthesis gas (H_2/CO=2). Compared with Fe-Si oxide, Fe-Si-Re oxide shows a lower CH_4 formation rate and a longer induction period. Since Re_2O_7 is reduced to Re at temperatures higher than 580 K, Re is likely to remain as the oxide during FTS at 523 K. Therefore, the addition of Re adversely inhibits the reduction and carburization of Fe-Si oxide at the reaction condition. Therefore, Re does not to give significant promotion effect on Fe-Si oxide catalyst and lead to higher FTS rates.

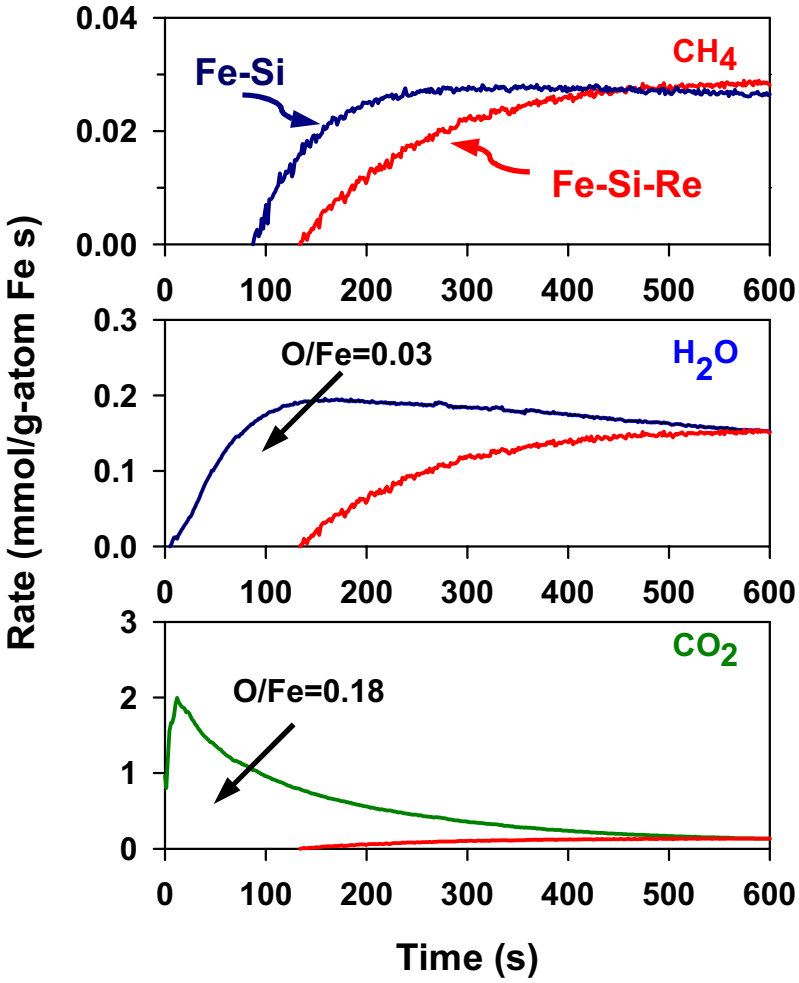

Figure 1.10 Comparison of the isothermal product transients of Fe_2O_3 and Fe-Si-Re oxide (0.2g, Si/Fe=0.046, Re/Fe=0.01) in synthesis gas (H_2/CO=2, 60 % synthesis gas in Ar, total flow rate 100 cm^3/min) at 523 K.

4. Fischer-Tropsch Synthesis over Fe-Si- based catalysts

4.1. Catalyst Loading and Activation

During this reporting period, Fe-Si-based catalysts were tested for the FTS reaction at a H_2/CO ratio of 2:1. The catalyst sample (80-140 mesh, 0.264 g) was diluted with quartz chips in order to avoid temperature gradients. The quartz chips were washed with diluted nitric acid and treated in air at 600 ^oC. The total bed volume, including catalyst and quartz chips, was 8 cm^3 to give a bed height of 8 cm. Temperatures were recorded along the catalyst bed during FT synthesis. It was found that temperatures were within ±0.5 ^oC of the average axial temperature and the average axial temperature was within ±0.2 ^oC of the desired setpoint. For all runs, the catalyst was activated before FT synthesis reaction. The activation procedure followed for the Fe-Si catalysts was different from the one used for the Fe-Zn catalysts. Activation was carried out *in situ* by heating the catalyst in a mixture of 81.5% CO and 18.5 % N_2 at 14.7 atm (12 atm CO) by increasing the temperature from 20 ^oC to 270 ^oC at a rate of 2 ^oC/min and holding it at 270^oC for a period of 24 hours. The more severe activation procedure was provided by Dr. B. H. Davis and it was necessary in order to complete the slower carburization of the Fe-Si and Fe-Si-K samples. Following this step, the reactor temperature and pressure were set to the desired reaction conditions.

4.2. Comparison between Fe-Zn-Cu-K and Fe-Si-K catalysts

The FTS reaction was carried out on a Fe-Si-K catalyst (Si/Fe=0.046, K/M=0.014) and its catalytic properties are compared in this section with a Fe-Zn-Cu-K (Zn/Fe=0.1, Cu/M=0.01, K/M=0.02) catalyst that was studied previously [19]. CO conversions on these two catalysts as a function of the reciprocal CO space velocity collected at 235^oC and 21.4 atm are shown in Fig. 1.11. The Fe-Si-K exhibits a higher activity for FTS reaction than Fe-Zn-Cu-K at a given value of space velocity.

During FTS, CO_2 can be formed *via* water-gas shift reactions (secondary CO_2 formation) and *via* removal of oxygen formed in the CO activation steps, using CO to form CO_2 (primary CO_2 formation). The CO_2 selectivities are shown as a function of the CO conversion on the two catalysts in Fig. 1.12. The CO_2 selectivity increased linearly with CO conversion and it was higher on Fe-Zn-Cu-K than Fe-Si-K. However, it is also observed that the slopes of the CO_2 selectivity curves are almost identical on the two catalysts, but the y-intercept is much higher on the Fe-Zn-Cu-K catalyst. Thus, it can be interpreted that the difference between the two catalysts lies mainly in the primary rates of CO_2 formation. The presence of Cu appears to favor the removal of surface oxygen as CO_2.

A comparison of methane selectivities on the two catalysts is shown as a function of CO conversion in Fig. 1.13. The methane selectivity is higher on Fe-Si-K. The C_{5+} selectivities were higher on Fe-Zn-Cu-K (Fig. 1.14).

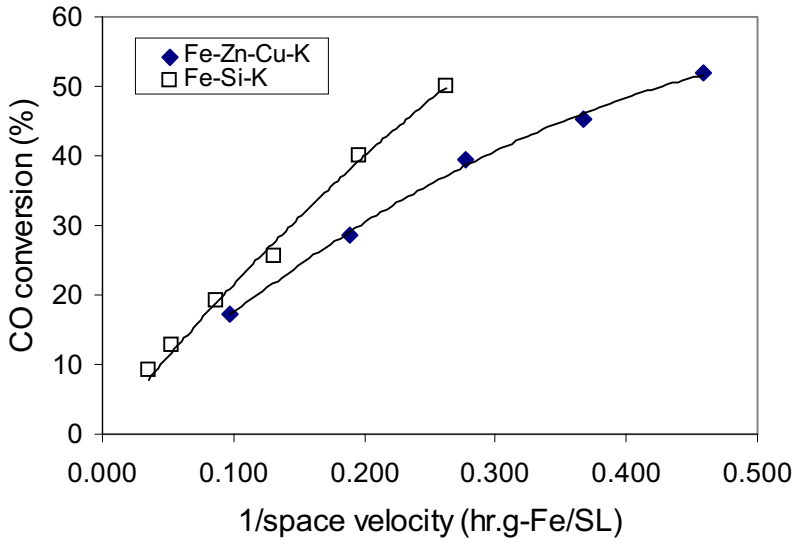

Fig. 1.11. CO conversion as a function of reciprocal space velocity for the Fe-Si (Si/Fe=0.046, K/Fe=0.014) and Fe-Zn-Cu-K (Zn/Fe=0.1, Cu/M=0.01, K/M=0.02) catalysts at 235^{o}C and 21.4 atm, H_2/CO=2.

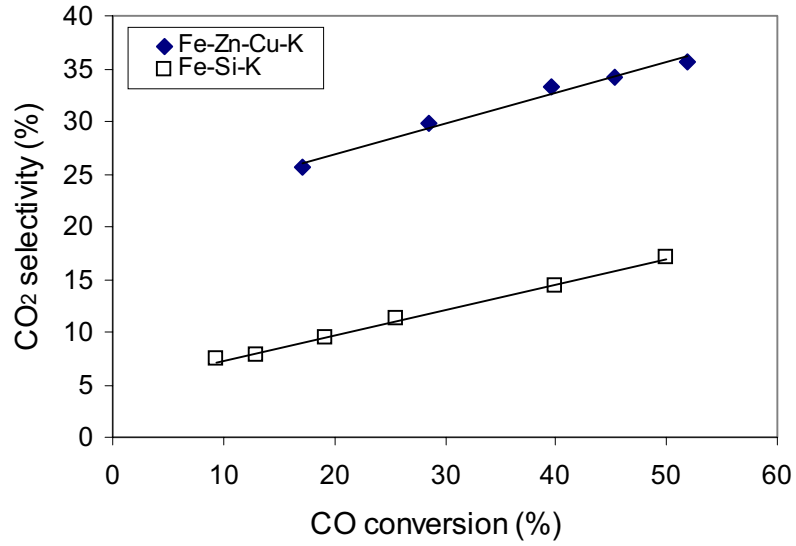

Fig. 1.12. CO_2 selectivity as a function of CO conversion over the Fe-Si (Si/Fe=0.046, K/Fe=0.014) and Fe-Zn-Cu-K (Zn/Fe=0.1, Cu/M=0.01, K/M=0.02) catalysts at 235^{o}C and 21.4 atm, H_2/CO=2.

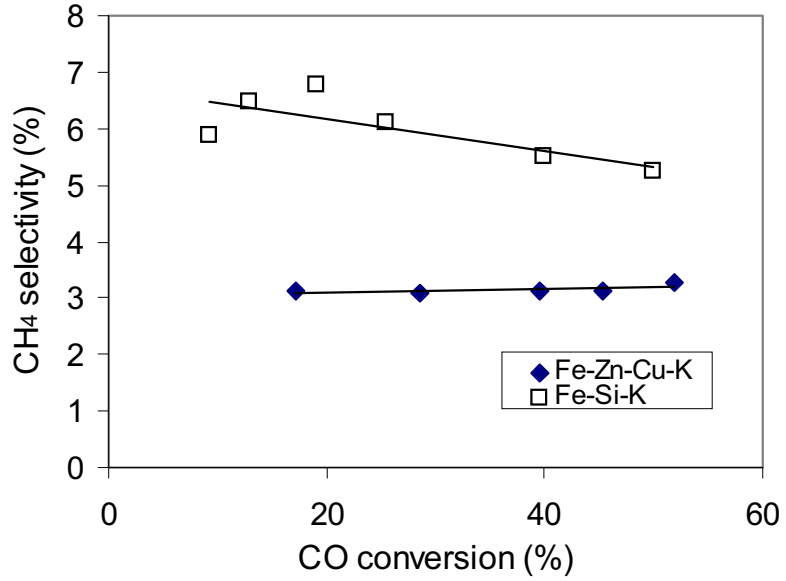

Fig. 1.13. CH_4 selectivity as a function of CO conversion over the Fe-Si (Si/Fe=0.046, K/Fe=0.014) and Fe-Zn-Cu-K (Zn/Fe=0.1, Cu/M=0.01, K/M=0.02) catalysts at 235°C and 21.4 atm, H_2/CO=2.

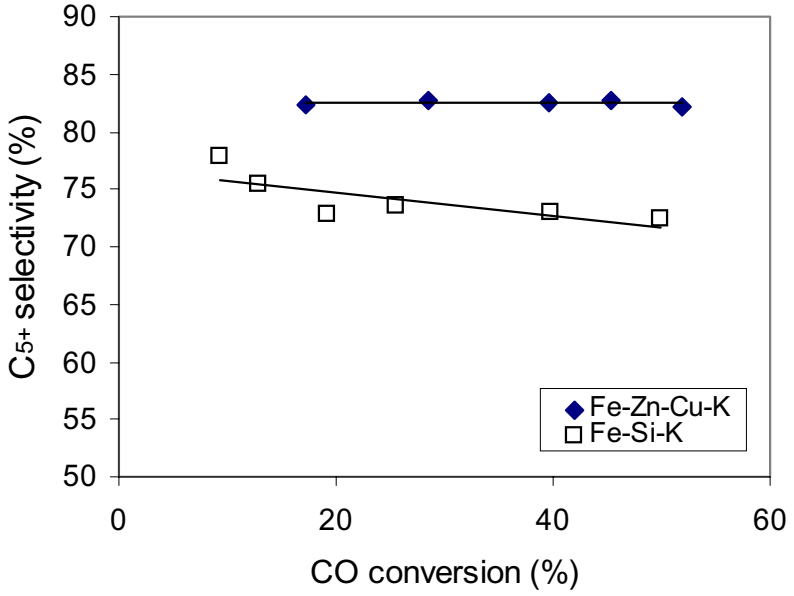

Fig. 1.14. C_{5+} selectivity as a function of CO conversion over the Fe-Si (Si/Fe=0.046, K/Fe=0.014) and Fe-Zn-Cu-K (Zn/Fe=0.1, Cu/M=0.01, K/M=0.02) catalysts at 235°C and 21.4 atm, H_2/CO=2.

Primary α-olefin products undergo secondary hydrogenation to form *n*-paraffins. The hydrogenation ability of α-olefin decreases with increasing carbon number, while the residence time of α-olefins within the catalyst pellets increases with increasing carbon number because of transport restrictions and hence olefins with higher carbon number have a greater chance to hydrogenate. Thus, the α-olefin/*n*-paraffin ratio is determined by

the balance between hydrogenation activity and the residence time of the α-olefins. The 1-butene/n-butane ratio for the two catalysts at 235°C and 21.4 atm are shown in Fig. 1.15 as a function of reciprocal CO space velocities. Both catalysts had a 1-butene/*n*-butane ratio that was almost unchanged with space time. The y-intercept of this curve is a measure of the intrinsic olefin-paraffin termination while the slope of the curve is a measure of the secondary hydrogenation/readsorption and chain growth. The slope of the curves for both catalysts was almost zero indicating that the catalysts exhibit no secondary hydrogenation reactions, due to the presence of K on the catalysts. The y-intercept was also almost the same for both the catalysts indicating no change in the intrinsic olefin-paraffin termination characteristics.

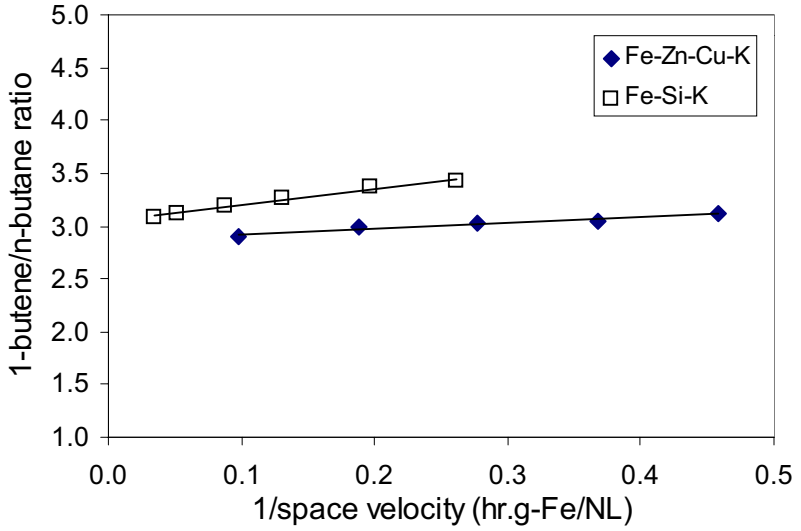

Fig. 1.15. α-Butene/n-butane ratio as a function of reciprocal space velocity for the Fe-Si (Si/Fe=0.046, K/Fe=0.014) and Fe-Zn-Cu-K (Zn/Fe=0.1, Cu/M=0.01, K/M=0.02) catalysts at 235°C and 21.4 atm, H_2/CO=2.

In the case of FTS reactions, the chain growth probability determines the carbon number product distribution. The hydrocarbon selectivities plotted in a semi-logarithmic scale as a function of the carbon number, on Fe-Si-K and Fe-Zn-Cu-K at 235°C and 21.4 atm, at similar CO conversions, are shown in Fig. 1.16. The selectivities decrease monotonically with carbon number and the plot gives a straight-line fit confirming that the product distribution is consistent with Flory polymerization kinetics with a single chain growth probability value of approximately 0.7. These results suggest that the chain growth probability is independent of the bed residence times and that readsorption of α-olefins and chain initiation do not strongly influence the product molecular weight distribution on these Fe-based catalysts.

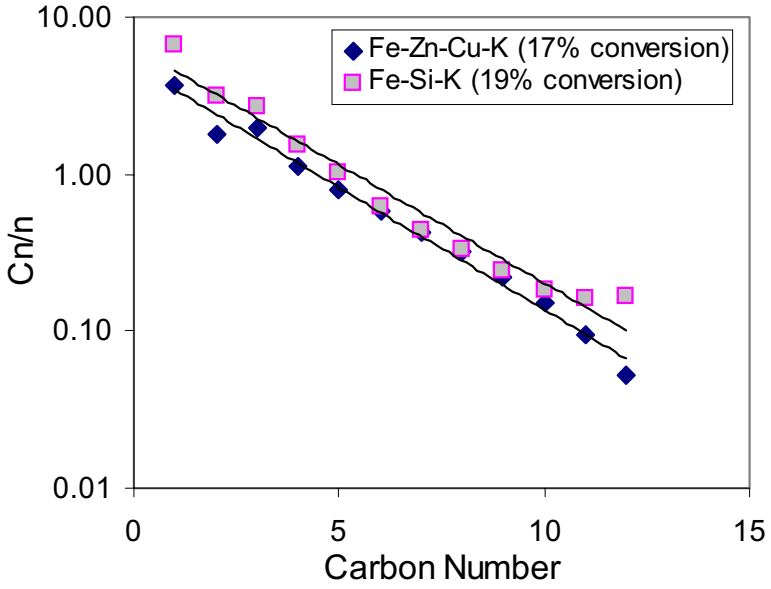

Fig. 1.16. Hydrocarbon selectivity as a function of the carbon number on the Fe-Si (Si/Fe=0.046, K/Fe=0.014) and Fe-Zn-Cu-K (Zn/Fe=0.1, Cu/M=0.01, K/M=0.02) catalysts at 235°C and 21.4 atm, $H_2/CO=2$.

4.3. Investigation of Potassium effects during FTS reaction

The addition of potassium has been found to influence the Fischer-Tropsch synthesis and the water-gas shift reaction rates and the product molecular weight on Fe-based catalysts. During this reporting period, the potassium effects on methane and higher hydrocarbon selectivities, the rates of the water-gas shift and Fischer-Tropsch synthesis, and the olefin selectivity were measured on Fe-Si catalysts with and without K (Si/Fe=0.046, K/Fe=0 and 0.014) several standard temperature and pressure conditions using synthesis gas with a H_2/CO ratio of 2:1.

4.3.1 Effects of Potassium on the Fischer-Tropsch Synthesis Activity

Previous studies on FT synthesis on Fe-based catalysts have shown that the presence of K increases the FTS and water-gas shift rates [14,17,19,23]. Potassium donates electrons to iron, thus increasing CO chemisorption energies, because CO draws electron density away from Fe atoms. In contrast, hydrogen donates electrons to iron (electron affinity decreases upon H_2 chemisorption), and the presence of electron-donating alkali should weaken Fe-H bonds. The net result of potassium promotion is the strengthening of the Fe-C bond and the weakening of C-O and Fe-H bonds [24]. The weakening of C-O bond favors its dissociation and the removal of oxygen by hydrogen to form $-CH_x$ monomers, an essential step in FTS catalytic sequence.

CO conversions on Fe-Si and Fe-Si-K at 235 °C and 21.4 atm are shown as a function of reciprocal CO space velocities in Fig. 1.17. The K-free catalyst showed a slightly higher

CO conversion than the K-promoted catalyst at the same CO space velocity. A similar result is observed at 220°C and 30 atm (Fig. 1.18). This result is in contrast to our findings on the effect of K-addition on Fe-Zn-Cu catalysts [19]. However, studies by O'Brien *et al.* on similar catalysts have shown that the addition of K to Fe-Si does not cause a significant change in the CO conversion [25]. However, their experiments were conducted with coal-derived syngas (with a H_2/CO ratio of 0.67). Since the H_2/CO ratio was higher in our case, the higher hydrogen availability at the surface should lead to higher CO rates (due to the positive dependence of the rate constant on the hydrogen concentration). In addition, our TPSR studies on Fe-Si catalysts presented in Section 3.5 show no significant change in the methanation rates upon K addition. Since K favors CO chemisorption and reduces H_2 chemisorption, the lack of a surface additive such as Cu to promote the dissociation of H_2, may lead to an unfavorable H_2/CO ratio on the catalyst surface, which could account for the lack of promotion of the FT rates.

Figures 1.19 and 1.20 show the CO rates and hydrocarbon formation rates at 235°C and 21.4 atm as a function of the reciprocal space velocity. At the same CO space velocity, CO conversion rates are higher on the K-free catalysts than on the K-promoted catalysts. The CO conversion rates decreased with increasing conversion for both the catalysts. The difference in the CO rates decreased with increasing CO conversion. Similar trends were observed for the hydrocarbon formation rates on the two catalysts (Fig. 1.20). These results point out to the lack of a K-promotion effect.

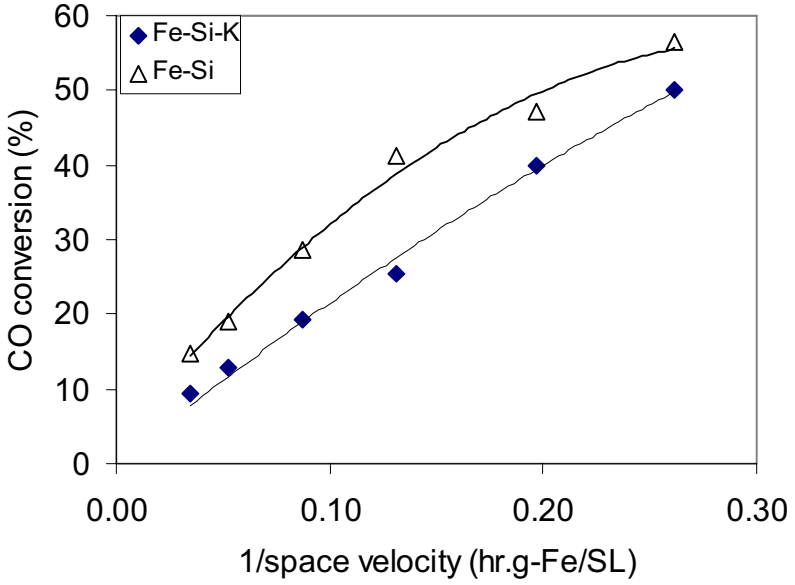

Fig. 1.17. CO conversion as a function of the reciprocal space velocity (Si/Fe=0.046, K/Fe=0 or 0.014) at 235 °C and 21.4 atm, H_2/CO=2.

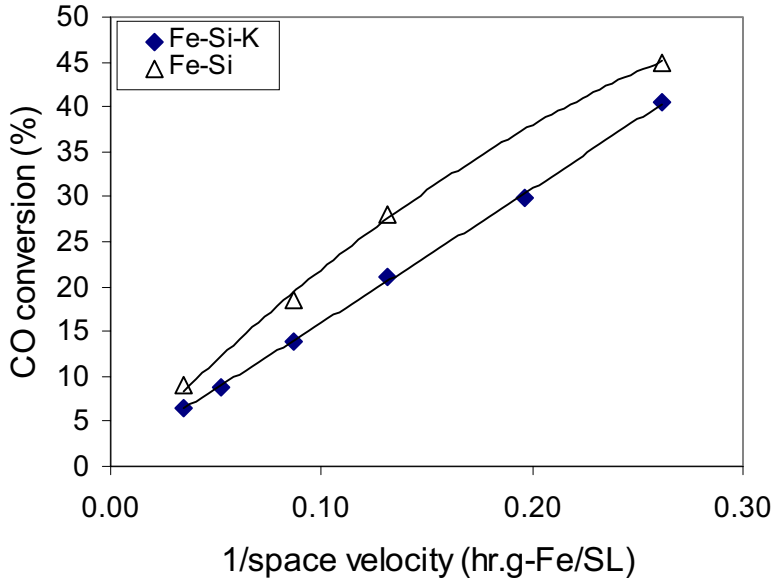

Fig. 1.18. CO conversion as a function of the reciprocal space velocity (Si/Fe=0.046, K/Fe=0 or 0.014) at 220 ^{o}C and 30 atm, H_2/CO=2.

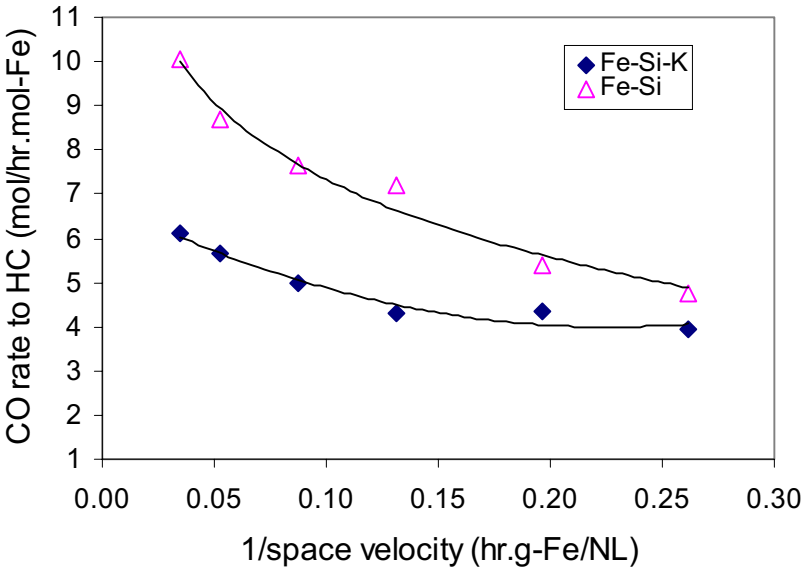

Fig. 1.19. CO rate as a function of reciprocal space velocity (Si/Fe=0.046, K/Fe=0 or 0.014) at 235^{o}C and 21.4 atm, H_2/CO=2.

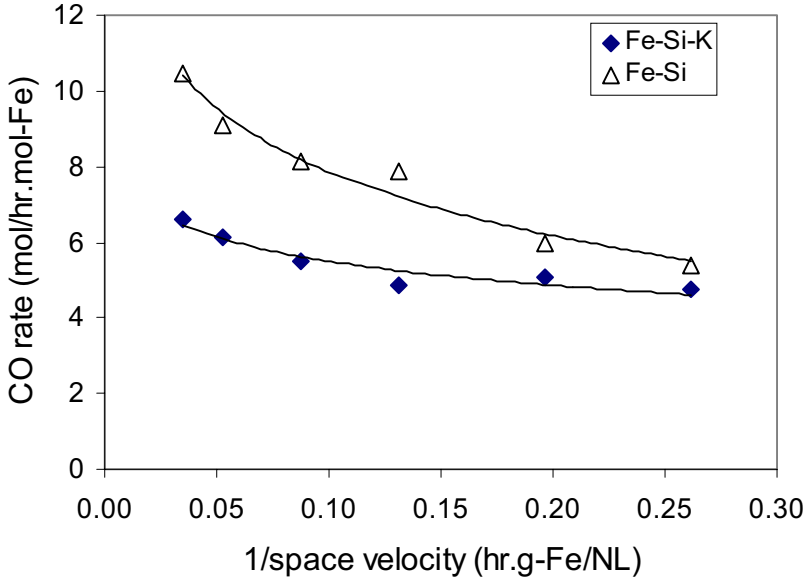

Fig. 1.20. Hydrocarbon formation rate as a function of reciprocal space velocity (Si/Fe=0.046, K/Fe=0 or 0.014) at 235 ^{o}C and 21.4 atm, $H_2/CO=2$.

4.3.2. Effects of Potassium on CO_2 selectivity

Water and CO_2 are both primary oxygenate products of the FT synthesis, but CO_2 can also form *via* subsequent secondary water-gas shift reactions. CO_2 can be formed in the primary steps *via* the removal of oxygen atoms from the catalyst surface using CO after the CO dissociation step that forms the -CH_x monomers.

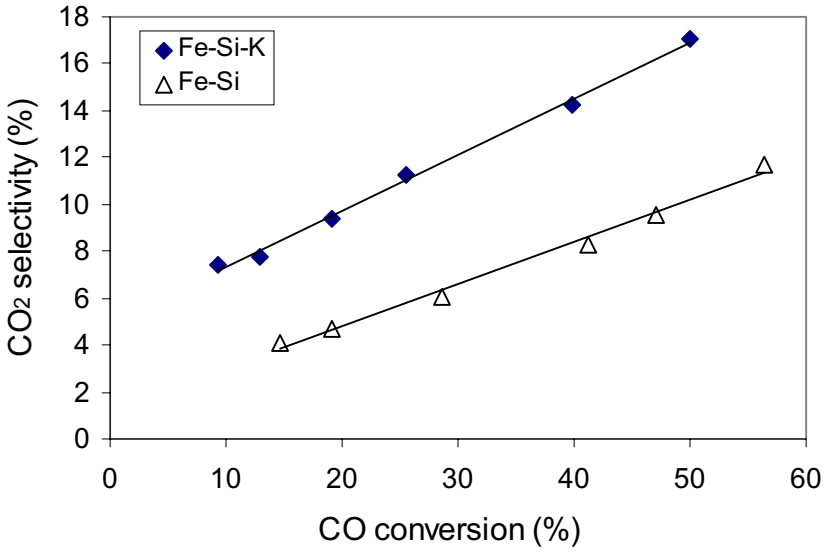

Fig. 1.21. CO_2 selectivity as a function of CO conversion on the catalysts (Si/Fe=0.046, K/Fe=0 or 0.014) at 235 ^{o}C and 21.4 atm, $H_2/CO=2$.

The CO_2 selectivity on the K-free and K-promoted Fe-Si catalysts is shown as a function of CO conversion at 235 ^oC and 21.4 atm in Fig. 1.21. The CO_2 selectivity increased with CO conversion on both catalysts. The CO_2 selectivity increased upon addition of potassium. The slope of the CO_2 selectivity curve is a measure of the secondary water-gas shift reaction while the y-intercept is a measure of the primary CO_2 removal rate, *via* the removal of oxygen formed in the CO dissociation step by CO as CO_2. Since the slopes of the two curves were almost identical but the y-intercepts were different, the addition of K to Fe-Si appears to favor the primary removal of surface oxygen as CO_2. The secondary water-gas shift reaction rate appears to be unaffected by the presence of K. However the increase in the CO_2 selectivity with K-addition was smaller in the case of Fe-Si (about 4% at ~19% CO conversion) compared to Fe-Zn-Cu catalysts (about 18% at ~20% CO conversion) indicating that these K-effects are smaller in the case of Fe-Si [19].

4.3.3. Effects of Potassium on Hydrocarbon Selectivity and 1-Olefin to *n*-Paraffin Ratio

Methane selectivities on the K-free and the K-promoted Fe-Si catalysts are shown as a function of CO conversion in Fig. 1.22. The methane selectivity was almost independent of CO conversion on K-promoted Fe-Si, while on K-free Fe-Si, the methane selectivity decreased slightly with increase in the CO conversion. The lower CH_4 selectivity in the presence of K in the Fe-Si catalyst observed in Fig. 1.22, indicates that potassium inhibits the formation of methane.

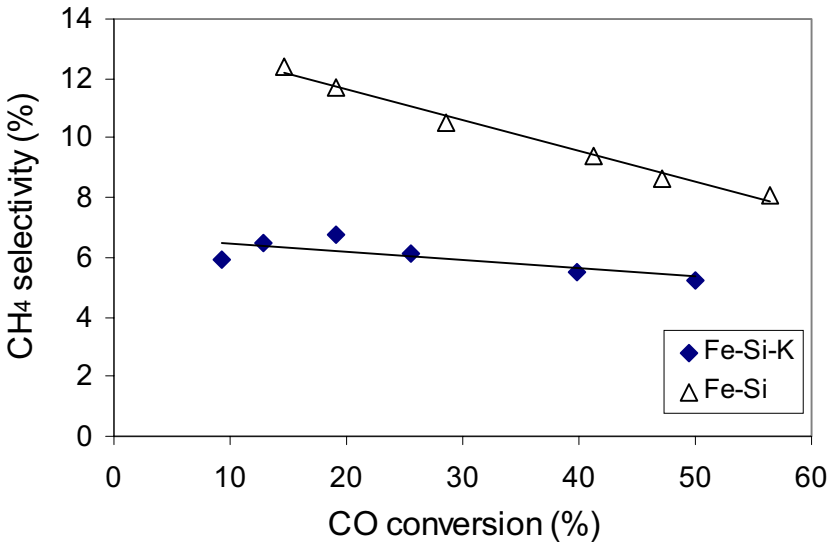

Fig. 1.22. Methane selectivity as a function of CO conversion on the catalysts (Si/Fe=0.046, K/Fe = 0 or 0.014) at 235 ^oC and 21.4 atm, $H_2/CO=2$.

The C_{5+} selectivities on Fe-Si and Fe-Si-K are compared at 235^oC and 21.4 atm as a function of CO conversion in Figure 1.23. The values are higher for Fe-Si-K than Fe-Si. The lower CH_4 selectivities and higher C_{5+} selectivity numbers appear to reflect the higher CO and lower hydrogen surface coverages in the presence of potassium, which

would lead to increased chain growth. K promotes CO chemisorption and prevents H_2 chemisorption on the catalyst surface. However, these effects are much smaller on Fe-Si than the Fe-Zn catalysts studied previously [19].

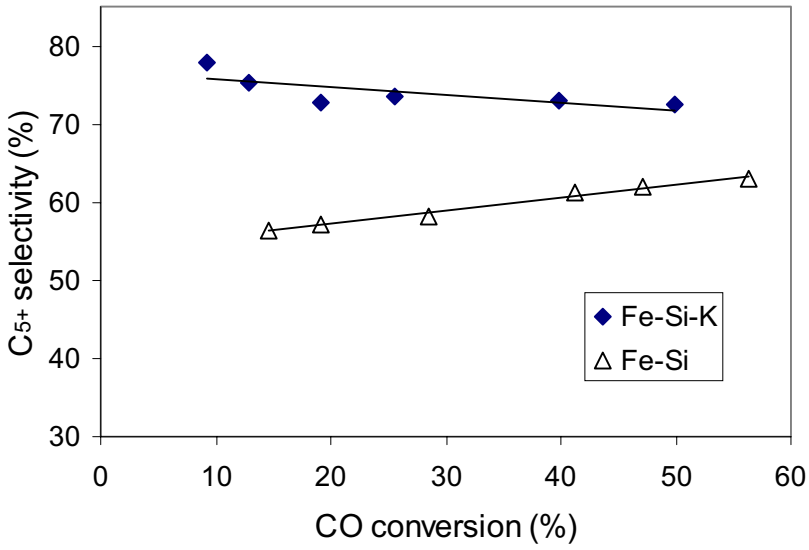

Fig. 1.23. C_{5+} selectivity as a function of CO conversion on the catalysts (Si/Fe=0.046, K/Fe=0 or 0.014) at 235 ^{o}C and 21.4 atm, H_2/CO=2.

During FT synthesis, hydrocarbon chains terminate either by hydrogen abstraction to form 1-olefins or by hydrogen addition to form *n*-paraffins [26]. In addition, 1-olefins can also undergo secondary hydrogenation reactions to form *n*-paraffins and secondary isomerization reactions to form branched olefin isomers.

The selectivity to various C_5 hydrocarbons is shown as a function of CO conversion on Fe-Si-K in Fig. 1.24 and on Fe-Si in Fig. 1.25. The slopes of the 2-pentene and 1-pentane selectivity curves were almost independent of CO conversion over both catalysts. This indicated that no secondary hydrogenation or isomerization reactions take place on these Fe-Si and Fe-Si-K catalysts. At low CO conversions, the 1-pentene selectivity was lower on Fe-Si-K than Fe-Si-K while at the higher CO conversions, the values approached each other. The y-intercept of the 1-pentane selectivity curve was lower for Fe-Si-K than Fe-Si indicating that the intrinsic termination to paraffins in the case of the K-promoted catalyst was much lower. The higher selectivity to olefins at higher CO conversions, indicate the preferential formation of olefins by β-hydrogen abstraction rather than paraffins by H-addition at these conditions. This also suggests that the termination of the hydrocarbon chains by H-addition is inhibited at higher CO conversion. This unique behavior is being investigated further.

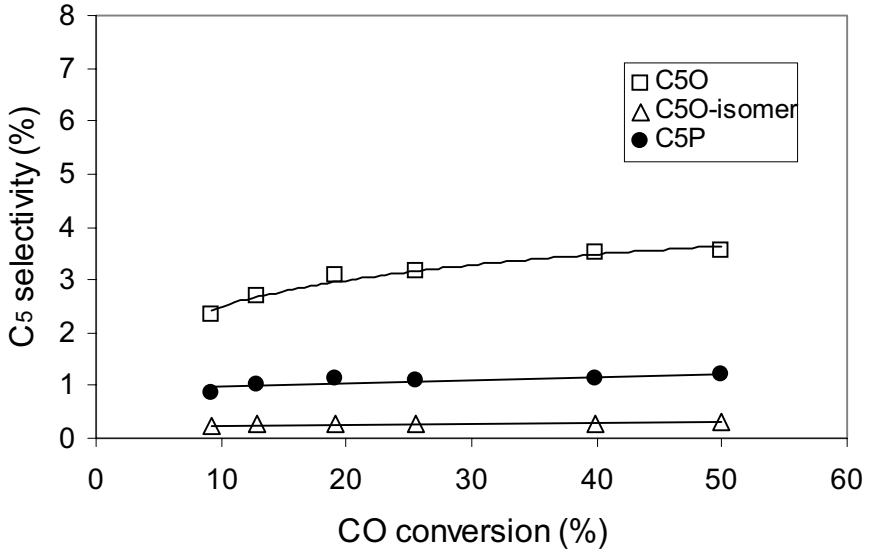

Fig. 1.24. The selectivities of C_5 hydrocarbons as a function of CO conversion on the Fe-Si-K catalyst (Si/Fe=0.046, K/Fe=0.014) at 235 ^{o}C and 21.4 atm, H_2/CO=2.

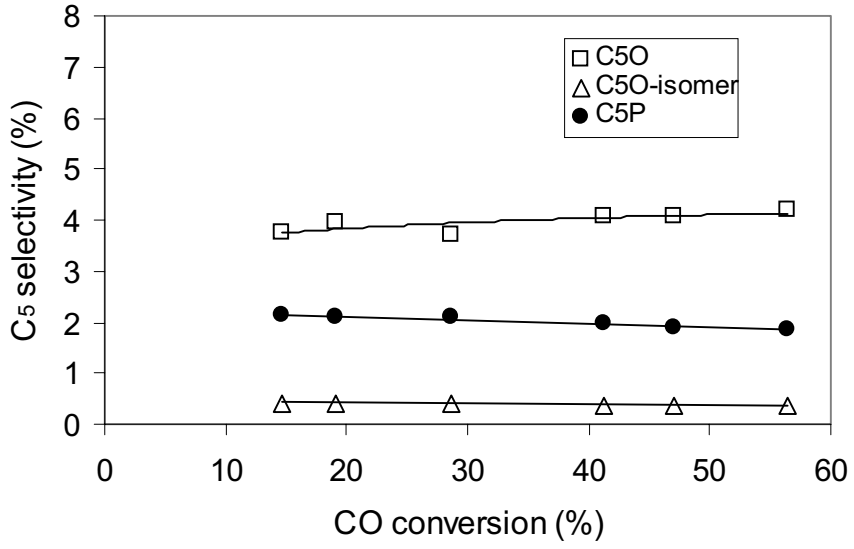

Fig. 1.25. The selectivities of C_5 hydrocarbons as a function of CO conversion on the Fe-Si catalyst (Si/Fe=0.046) at 235 ^{o}C and 21.4 atm, H_2/CO=2.

II. FISCHER-TROPSCH SYNTHESIS ON COBALT CATALYSTS

1. Catalyst Loading, Activation and Experimental conditions

During this reporting period, FTS experiments were conducted on a 21.9% Co/SiO_2 catalyst as part of our continuing efforts to certify the re-designed reactor unit. The experiments were performed with 1.06 g of catalyst diluted with 2.8 g of SiO_2 in order to avoid any temperature gradients caused by the exothermic nature of the reaction. The activation procedure was identical to that used previously and it has been described in detail in an earlier report [19]. Runs were conducted at 200°C and 20 atm at several space velocities. The addition of water at different partial pressures (2 atm, 4 atm and 6 atm) was also studied at constant partial pressures of CO and H_2.

2. Comparison of Activity and Selectivity Data

FTS site-time yields on 21.9% Co/SiO_2 catalyst obtained in our space velocity and water addition runs are shown in Fig. 1.25 as a function of the water partial pressure. The site-time yield data obtained previously in the same unit are also shown in Fig. 1.26. These site-time yields were similar in all runs.

CH_4 selectivities obtained in both cases are also shown in Figure 1.27 as a function of the water partial pressure. The CH_4 selectivities obtained recently were higher than those reported previously, especially at low space times. Similarly, the C_{5+} selectivities are shown in Figure 1.28 as a function the water partial pressure. The C_{5+} selectivities were lower in the most recent experiments than in those reported earlier.

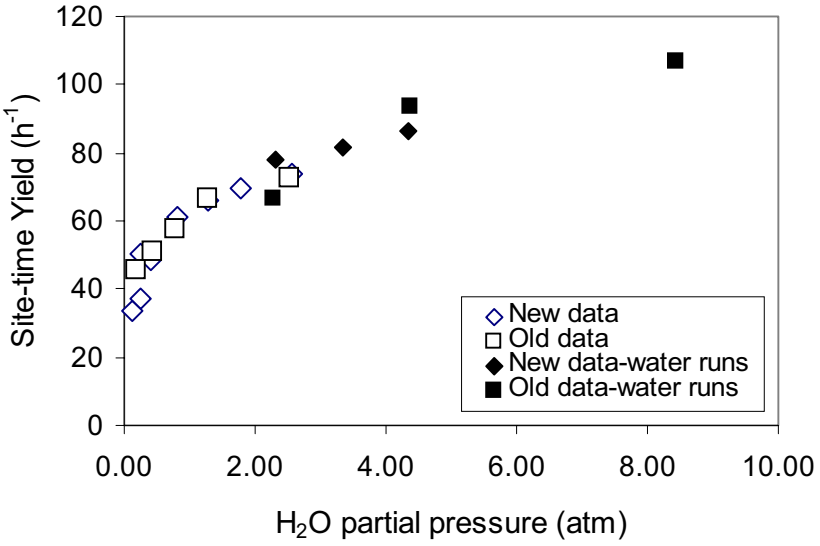

Figure 1.26. A comparison of the site-time yield data for the 21.9% Co/SiO_2 catalyst obtained at 200°C and 20 atm, $H_2/CO=2$.

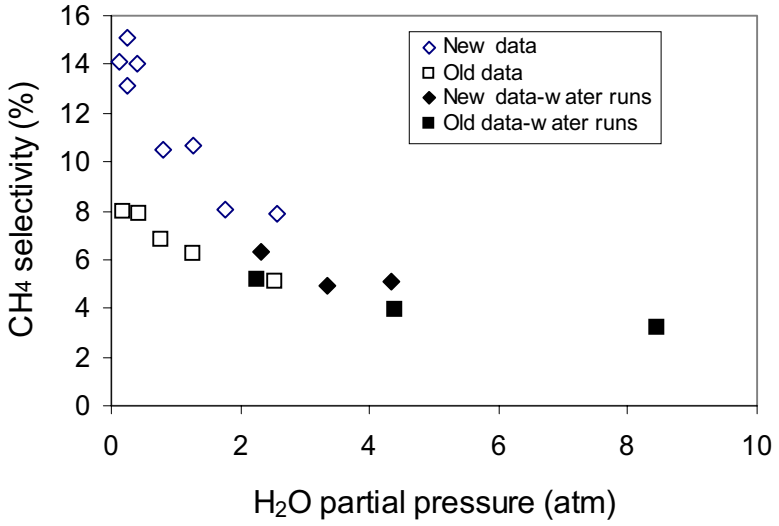

Figure 1.27. A comparison of the CH_4 selectivities as a function of H_2O partial pressure for the 21.9% Co/SiO_2 catalyst at 200°C, 20 atm, $H_2/CO=2$.

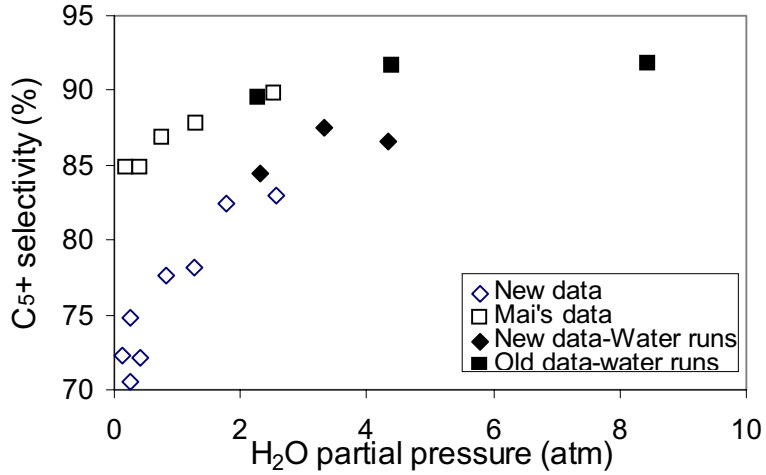

Figure 1.28. A comparison of the C_{5+} selectivities as a function of H_2O partial pressure for the 21.9% Co/SiO_2 catalyst at 200°C, 20 atm, $H_2/CO=2$.

α-Olefin/n-paraffin ratios obtained at a space velocity of 90 cc/g/min are shown in Figure 1.29 as a function of carbon number. It can be observed that the O/P ratios are lower in the newer data indicating a higher hydrogenation tendency than in the previous runs. This is consistent with the higher CH_4 selectivities observed in the recent experiments. These experiments were repeated after higher pre-treatment (reduction) temperatures (325°C and 350°C) in order to make sure that the differences did not arise from incomplete reduction of the catalyst. The site-time yields in both these cases were identical to the ones obtained previously. C_{5+} selectivities were higher than the values obtained after

reduction at 300°C, but still lower than those in the earlier experiments (Figure 1.30). α-Olefin/n-paraffin ratios also increased with increasing reduction temperature.

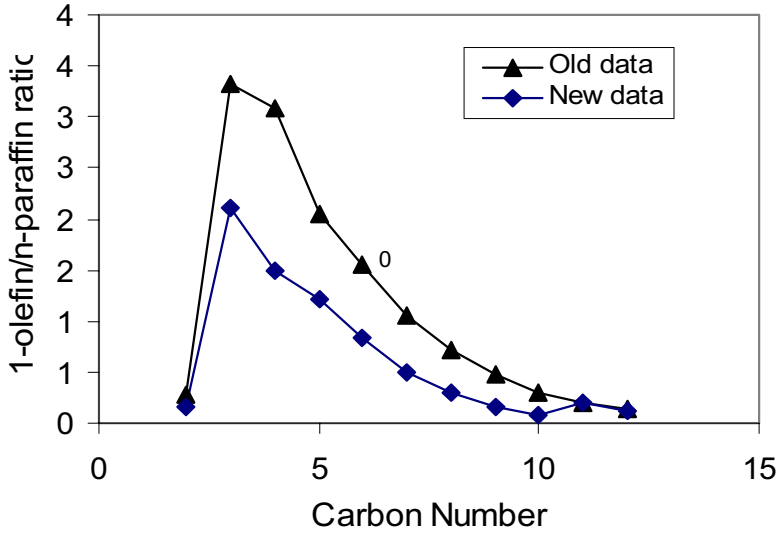

Figure 1.29. 1-Olefin/n-paraffin ratios obtained at a space velocity of 90 cc/g/min in both the data sets with the 21.9% Co/SiO_2 catalyst at 200°C, 20 atm, $H_2/CO=2$.

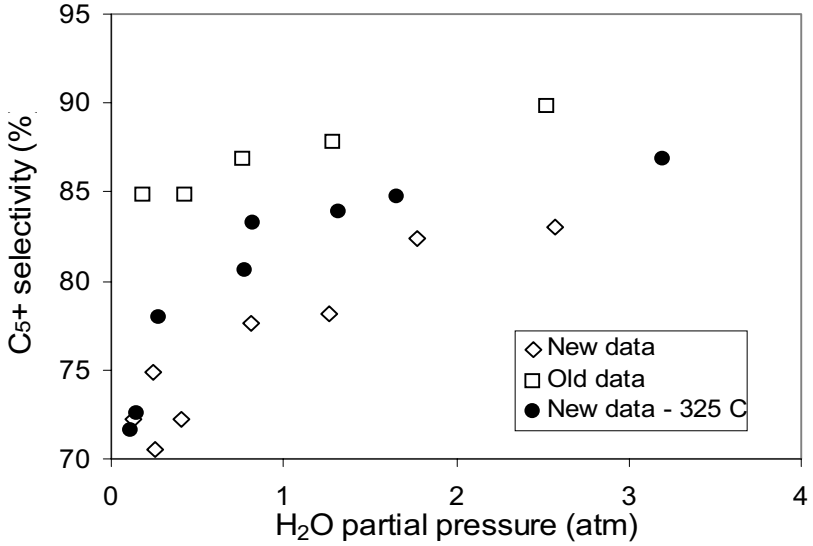

Figure 1.30. A comparison of the C_{5+} selectivities with the different pretreatment temperatures as a function of H_2O partial pressure for the 21.9% Co/SiO_2 catalyst at 200°C, 20 atm, $H_2/CO=2$.

Further increases in the pretreatment temperature from 325°C to 350°C did not influence the α-Olefin/1-paraffin ratios, and the C_{5+} or CH_4 selectivities. A number of experimental parameters are being examined as possible causes of the discrepancies in the data. These

parameters include recalibration of the response factors in the TCD and FID chromatograms that could eliminate any errors in calculation of the selectivities, confirmation of the H_2/CO ratio reported by the supplier for the gas mixture used in the experiments and the possibility of hydrogenation on the walls of the reactor.

3. Analysis and Regression of Data

Most of the effort during this quarter was spent developing a program to fit the reaction data obtained previously to postulated rate laws. Work continues on a program capable of fitting data to an arbitrary rate expression. This program is expected to be complete in the next quarter and it will be used to help design our next set of kinetic experiments as well as validate our proposed rate expressions.

II. APPENDIX

1. References

1. M. E. Dry, The Fisher-Tropsch Synthesis, in *Catalysis-Science and Technology*, Vol. 1, p. 160, J. R. Anderson and M. Boudart eds., Springer Verlag, New York, 1981.
2. F. Fischer and H. Tropsch, *Brennstoff-Chem.* 7 (1926) 97.
3. R. B. Anderson, in *Catalysis* Vol. 4, p. 29, P. H. Emmett eds., Van Nostrand-Reinhold, New York, 1956.
4. H. H. Storch, N. Golumbic and R. B. Anderson, *The Fischer-Tropsch and Related Syntheses*, Wiley, New York, 1951; R. B. Anderson, *The Fischer-Tropsch Synthesis*, Wiley, New York, 1984.
5. H. Kolbel and M. Ralek, *Catal. Rev.-Sci. Eng.* 21 (1980) 225.
6. J. W. Niemantsverdriet and A. M. van der Kraan, *J. Catal.* 72 (1981) 385.
7. J. A. Amelse, J. B. Butt and L. J. Schwartz, *J. Phys. Chem.* 82 (1978) 558.
8. G. B. Raupp and W. N. Delgass, *J. Catal.* 58 (1979) 348.
9. R. Dictor and A. T. Bell, *J. Catal.* 97 (1986) 121.
10. J. P. Reymond, P. Meriaudeau and S. J. Teichner, *J. Catal.* 75 (1982) 39.
11. C. S. Kuivila, P. C. Stair and J. B. Butt, *J. Catal.* 118 (1989) 299.
12. C. S. Huang, L. Xu and B. H. Davis, *Fuel Sci. Tech. Int.* 11 (1993) 639.
13. S. Soled, E. Iglesia and R. A. Fiato, *Catal. Lett.* 7 (1990) 271.
14. S. Soled, E. Iglesia, S. Miseo, B. A. DeRites and R. A. Fiato, *Topics in Catal.* 2 (1995) 193.
15. E. Iglesia, A research proposal submitted to the Division of Fossil Energy.
16. R. J. O'Brien, L. Xu. R. L. Spicer and B. H. Davis, *Energy and Fuels*, 10 (1996) 921.
17. D. B. Bukur, D. Mukesh, and S. A. Patel, *Ind. Eng. Chem. Res*., 29, 194 (1990).
18. 4th Quarterly report, 1998. U.S. Department of Energy under contract # DE-FC26-98FT40308.
19. 1st Quarterly report, 1999. U.S. Department of Energy under contract # DE-FC26-98FT40308.
20. 2nd Quarterly report, 1999. U.S. Department of Energy under contract # DE-FC26-98FT40308.
21. 3rd Quarterly report, 1999. U.S. Department of Energy under contract # DE-FC26-98FT40308.
22. 4th Quarterly report, 1999. U.S. Department of Energy under contract # DE-FC26-98FT40308.
23. H. Kolbel, in Actes du Deuxieme Congres Internationale de Catalyse, Tchinp, Paris, 1960; Vol. II, 2075-2099.
24. J. Benziger, and R. Madix, *Surf. Sci. Catal*., 109 (1981) L527.
25. A. P. Raje, R. J. O'Brien, and B. H. Davis, *J. Catal*., 180 (1) (1998) 36.
26. R. C. Brady, and R. Pettit*, J. Am. Chem. Soc.*, 103 (1981) 1287.

Task 12. Reporting/Project Management

Three monthly and one quarterly reports have been completed.